Summary Scholar Report

## Summer Scholar Report

Bromination of anti-TGF-β1 for applications in imaging fatty liver via immuno-enhanced dual energy CT (eDECT)

John Ernandez,[1] Dr. Mark W. Grinstaff,* 1Department of Chemistry, *Departments of Chemistry and Biomedical Engineering, Boston University, Boston, MA 02215

Introduction:

Several methods of soft tissue visualization exist, yet few are capable of generating three-dimensional images of tissue morphology with quantitative information on composition and distribution of key artifacts. Enhanced single-energy computerized tomography (eSECT) has a history of use in visualization of whole or segmented embryos,[1] insects,[2] small mammals,[3] and reptiles[4] typically using X-ray active stain Lugol's iodine (see Figure 1a).
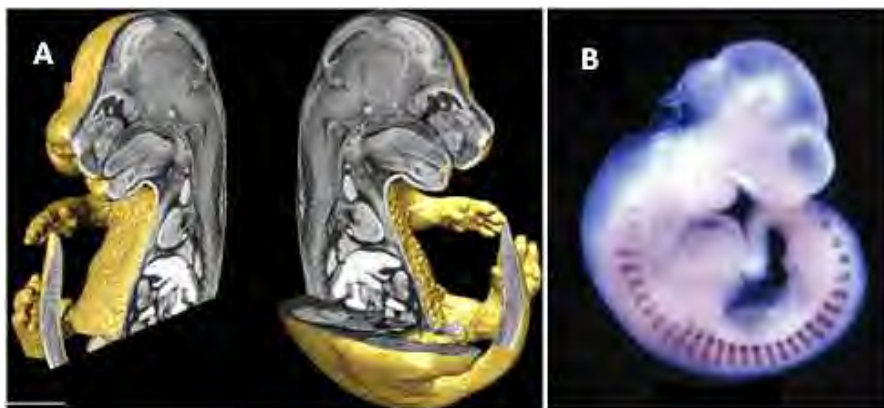
Figure 1a. Lugol-stained E15.5 stage mouse embryo imaged via eSECT with 3D projection-based reconstruction. 1b. Whole-mount in situ hybridization of myogenin expression in E10.5 mouse embryo.

Yet, eSECT does not allow for determination of chemical composition of stained samples. Similarly, whole-mount immunostaining may be used to determine the distribution of key biomarkers[5] and patterning defects[6], but only provides two-dimensional visualization (see Figure 1b). This project proposes immuno-eDECT which allows for visualization of soft tissue morphology and separation of artifacts in 3D using X-ray active brominated antibodies for key biomarkers. Dual energy CT hinges on the ability to exploit differences in atomic K-edge values in heterogeneous mixtures (Figure 2)[7] By bombarding a heterogeneous sample with X-ray energies specific for each component of the material, differences in resulting attenuation allow for "separation" of each component from the material.
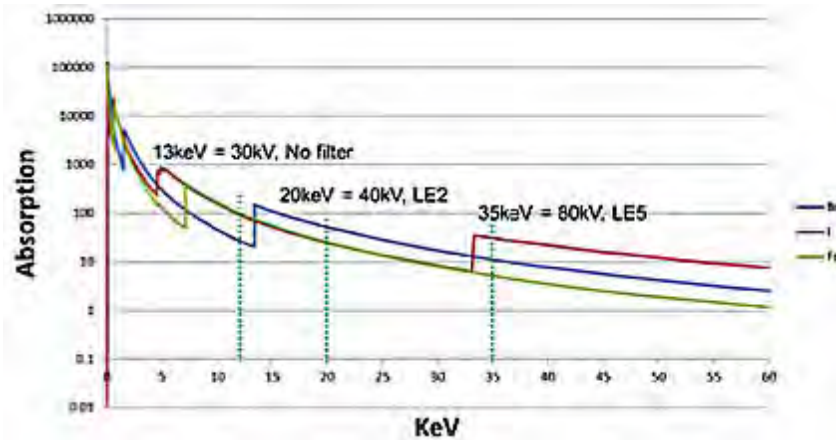
Figure 2. X-ray absorption of bromine, iodine, and iron. For example, bombarding a heterogeneous mixture of iodine and bromine with X-ray energy at 80 kV "separates" iodine content from bromine content based on differential absorption responses

This study focuses on validation and optimization of bromination of anti-TGF-β 1, an antibody specific for fibrosis biomarker TGF-β 1, and preliminary evaluation of immuno-eDECT. TGF is essential in the pathway towards liver fibrogenesis found in non-alcoholic fatty liver disease (NAFLD) where it regulates conversion of hepatic stellate cells (HSCs) into myofibroblasts (MFBs) and upregulates the generation of reactive oxygen species.[8-11] NAFLD impacts over 30 million Americans[12] and is historically evaluated using qualitative, categorical scoring which results in overestimation of key artifacts.[13-15] We believe that 3D visualization via eDECT with brominated biomarkers will improve upon previous challenges in resolving heterogeneous liver via unenhanced CT[16-17] while also allowing for more quantitative analysis of tissue.

Experimental Methods and Materials
Bovine serum albumin (BSA), N-bromosuccinimide (NBS), N-acetyl L-tryptophan methyl ester, N-acetyl L-tyrosine ethyl ester, guanidine-HCl, Coomassie Brilliant Blue, thioglycolic acid, phenol and solvents (including acetic acid, DMSO, and acetonitrile) were purchased from Sigma Aldrich. Lapine anti-TGF-β 1 was purchased from Abcam. HRP affinity isolated polyclonal swine anti-rabbit immunoglobulin was purchased from Agilent Technologies. Vector VIP peroxidase substrate was purchased from Vector Laboratories. Control and high fat diet C57 black male mice were received from and sacrificed by Jackson Laboratories. Bradford assay for protein fragmentation and ELISA were carried out using a Beckmann Coulter AD 340 Platereader. Tandem mass spectrometry was performed using Waters Tandem Quadrupole. Fourth derivative spectroscopy was carried out via HP Agilent diode array spectrophotometer. Sandwich ELISA was performed using Affymetrix eBioscience Ready-SET-Go! kit for human and

mouse TGF-β 1. Circular dichroism was performed on Applied Photophysics CS/2 Chirascan with accompanying software. Imaging of whole-mount immunostaining was performed with Olympus IX70 microscope with SPOT Insight Firewire camera.
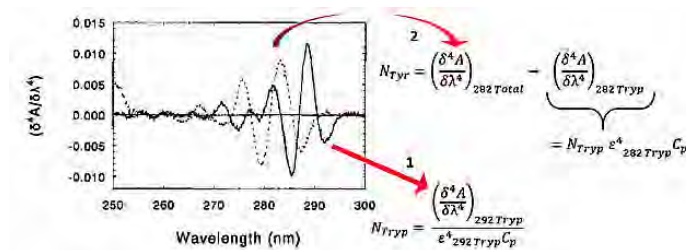
Direct protein bromination
Determination of optimal bromination time was carried out on BSA, adding 9 ml of 1 mg/ml BSA in phosphate-buffered saline (PBS) to 1 ml of 4 mM NBS, reacting at room temperature for 60 minutes, sampling and halting the reaction every 10 minutes by dialyzing in nanopure water at 4 °C for 48 hours with frequent bath changes. Dialysis bath content was centrifuged at 2500 rpm to concentrate and compared to a Bradford reagent calibration curve to determine degree of fragmentation due to oxidation. An aliquot of 0.25 mg/ml anti-TGF-β 1 was then brominated in 4 mM NBS for optimized time of 40 minutes at room temperature, also halted with dialysis for 48 hours. Optimization reactions varied NBS concentration to 8 and 12 mM and pH to 3.0 and 9.0 under similar conditions.

Tandem mass spectrometry
BSA and antibody samples were first lyophilized overnight. BSA was then degraded in 6 M hydrochloric acid (8 M for antibody) with 10 μL of 1 μg/ml phenol and 50 μL of thioglycolic acid at 105 °C for 16 hours (48 hours for antibody) in 40 ml pressure vials. Residual acid content was removed via lyophilization and amino acid residue was resuspended in 0.1% acetic acid. A gradient elution was performed as cited by Kato, et al.[18] Native and brominated tyrosine were used as standards.

Fourth derivative UV spectroscopy
UV analysis follows a method developed by Bray, et al[19] to determine the number of tyrosyl residues brominated by NBS. In brief, UV absorption due to tryptophan must first be quantified and separated from absorption due to tyrosine (see Figure 3). Aliquots ranging from 0.03 to 0.15 mM of tryptophan methyl ester standard are added to 6 M guanidine buffer and read from 250 to 310 nm, for determination of the tryptophan molar extinction coefficient at 282 and 292 nm, Then 1 mg/ml BSA and 2.2 μM antibody are spiked with aliquots of 4.9 and 1.0 μM tyrosine ethyl ester, respectively, to create standard additions plots from which the number of unaffected tyrosyl residues may be determined and subsequently the percent bromination.

$$N_{Tyr} = \left(\frac{\delta^4 A}{\delta \lambda^4}\right)_{282\,Total} - \underbrace{\left(\frac{\delta^4 A}{\delta \lambda^4}\right)_{282\,Tryp}}_{= N_{Tryp}\,\varepsilon^4{}_{282\,Tryp}\,C_p}$$

$$N_{Tryp} = \frac{\left(\frac{\delta^4 A}{\delta \lambda^4}\right)_{292\,Tryp}}{\varepsilon^4{}_{292\,Tryp}\,C_p}$$

Figure 3. *UV activity of most proteins is due to absorption from aromatic amino acids tyrosine and tryptophan. A characteristic peak at 282 nm represents an overlay of tyrosine and tryptophan absorption, whereas the characteristic 292 nm trough is solely tryptophan absorption. Equation 1 allows for calculation of tryptophan absorptivity at 292 nm, determined from tryptophan standards. Equation 2 then separates the contribution of tryptophan to the 282 nm absorption to quantify the number of intact tyrosyl residues.*

## Sandwich enzyme-linked immunosorbent assay (ELISA)

Seven wells across two rows of a Coulter 96-well plate were used to compare native and brominated antibody immunogenicity. Manufacturer-provided capture antibody, TGF antigen, HRP-linked secondary antibody and coloring reagent were used. Two-fold serial dilutions were performed on TGF antigen to create a calibration curve. The Lindmo method of infinite antigen excess[20] was used to determine immunogenicity.

Circular dichroism

Aliquots of 0.2 mg/ml of native and brominated BSA and antibody in PBS were scanned in triplicate with a 1 mm crystal cuvette ranging from 200 to 280 nm. Scans were performed over the course of days after bromination to monitor protein structural stability.

Validation of bromine and iodine X-ray separation

Solutions of 0.02 mM NBS and Lugol's iodine (equivalent to the maximum concentration of staining agent in murine liver) were loaded into roughly 1 cm polystyrene capillary tubes. A 1:1 mixture was also produced. The tubes were loaded into a specially designed polystyrene hollowed fixture which allows for minimal pixel shifting over the course of scanning (see Figure 4). Scanning was performed via Zeiss Xradia 520 Versa at 40 and 80 kVp, with LE2 and LE5 filters, for bromine and iodine respectively. Scanning occurred at roughly 4X magnification with 5 μm^3 isotropic resolution for 5 hours. Post-processing such as calibration to low- and high-attenuating standards, filtering, and masking was performed on Zeiss Reconstructor 11 and DSCoVer 11 software, with 3D reconstruction performed on Analyze (Mayo Clinic).
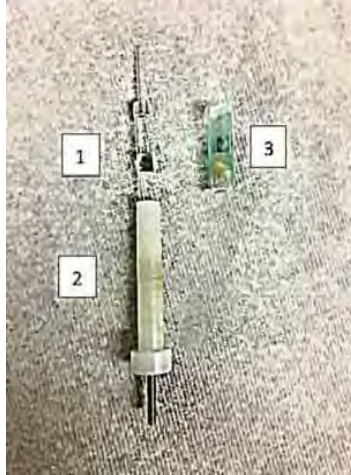
Figure 4. 1) Cylindrical sample holder customized for CT scanning with minimal pixel drift. 2) Sample platform insert which also serves as high-attenuating standard for calibration. 3) Samples are embedded in 0.5% agarose in plastic "plugs" and loaded on 2.

Lugol's iodine time course on ex vivo murine liver tissue

Five 0.5 cm sections of healthy murine tissue were first fixed overnight at 4 °C in Dent's fixative (80% methanol, 20% DMSO) and then underwent four freeze/thaw cycles at -80 °C in 100% methanol. Tissues were rehydrated in 50 and then 15% methanol and permeabilized for 30 minutes at room temperature with 10 μg/ml proteinase K. Sections were each stained under one of the five following conditions: 3, 18, and 24 hours at 0.3% Lugol and 42 hours 0.3% with 6 and 30 hours at 3.0% Lugol's. Sections were rinsed at the end of each staining period and cast in 0.5% agarose in small plastic cylinders (Figure 4). Sections were then scanned on Scanco μCT40 at 70 kVp with 3D reconstruction performed on Analyze (Mayo Clinic).

Whole-mount immunostaining and X-ray visualization of ex vivo murine liver tissue

Murine livers were dissected from 10% (control) and 60% fatty diet-fed mice and lobes separated into roughly 50 mg cubic sections. The whole-mount immunostaining protocol proposed by Sillitoe and Hawkes[21] was adopted with some modifications. Native and brominated antibody was incubated at 100-, 500-, and 1000-fold dilutions for 4 days. After 2 days of incubation of HRP-linked secondary antibody, sections were dehydrated in sucrose gradations, frozen in TissueTek, and cryosectioned into 20 μm slices followed by coloration with Vector VIP peroxidase substrate until proper signal-tonoise was achieved. Subsequent visualization was carried out via brightfield light microscopy. Optimal dilution factor 100x was applied to brominated antibody for 7 days on control and fatty liver sections followed by 3D visualization via Scanco μCT 40 as preliminary testing for immuno-eDECT.

Results

Direct protein bromination afforded low oxidative fragmentation with acceptable degrees of bromination. Bradford UV assay of dialysis bath content revealed protein fragmentation below 1%. Optimization reactions revealed that decreasing pH from 9.0 to 3.0 did significantly decrease bromination of BSA from 88 to 56%, while doubling or tripling NBS concentration had no significant impact on bromination (see Table 1) as determined by fourth-derivative assay. Fourth derivative spectroscopy predicted 16.8 ± 3.1 tyrosyl residues, agreeing with the 19 residues found in native BSA. It was determined that lapine anti-TGF used contained 15.9 ± 4.5 tyrosyl residues. As seen in Table 2, a significant difference in degree of bromination was seen with both BSA and antibody bromination in comparison to native forms, with 36% bromination of anti-TGF and 78% bromination of BSA, when bromination occurs at physiological pH 7.4.

Conditions	Tyr Brominated	Average Percent Bromination
pH 3.0†	10.7 ± 6.5	56
pH 7.4	14.8 ± 5.8	78
pH 9.0	16.7 ± 6.1	88
8 mM NBS	14.5 ± 5.1	76
12 mM NBS	15 ± 10	79

Table 1. *Impact of pH and NBS concentration on BSA tyrosyl bromination. Note that values marked with † show significant ($p < 0.05$) difference in the number of brominated tyrosyl residues than bromination at pH 7.4.*

| Protein of Interest	Calculated Tyr per Protein	Theoretical Tyr per Protein
Native BSA	16.8 ± 3.1	19
Brominated BSA	4.2 ± 5.8	
Native anti-TGF-β1	15.9 ± 4.5	≥9†
Brominated anti-TGF-β1	10.2 ± 8.5	

Table 2. *Number of tyrosine residues not brominated via oxidation as detected by UV spectroscopic assay. Note prediction of number of tyrosine residues in native BSA agrees with theory. Significant difference in tyrosine residues between native and brominated BSA ($p < 0.001$) and native and brominated antibody ($p = 0.002$). †Lapine Fc IgG, UniProt database.*

Tandem mass spectrometry revealed bromination of BSA in comparison to native and brominated tyrosine standards. Both monobromination (m/z 262 → 216) and substantial dibromination (339 → 293) of BSA is detected. Successful total acidic degradation of BSA is also noted by the presence of characteristic free tyrosyl degradation (182 → 136). (see Figure 5).
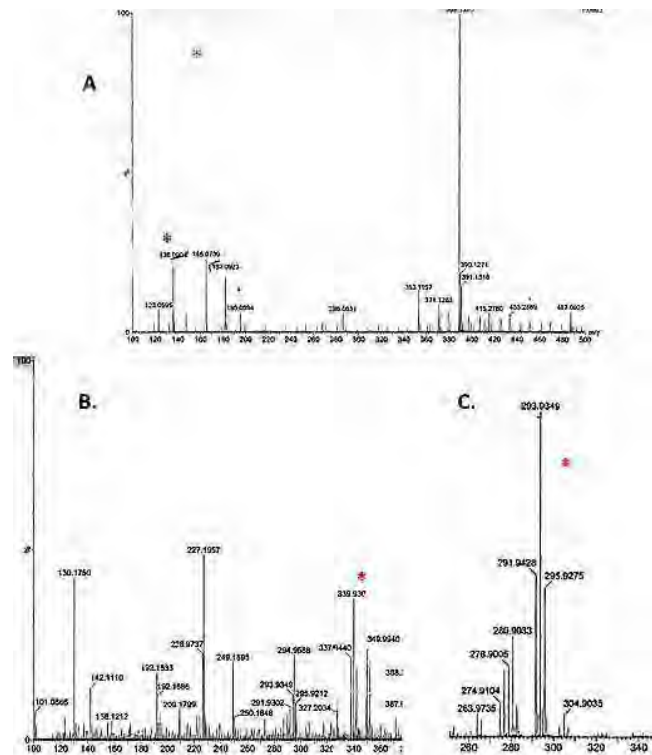
**Figure 5a.** *Tandem LC/MS of native BSA demonstrating successful total acid degradation with m/z 182 →136 tyrosine shift b. ESI LC/MS of brominated BSA demonstrating dibromination pattern at m/z 339 c. Tandem LC/MS of brominated BSA demonstrating dibrominated tyrosyl fragmentation of m/z 339 → 293. Note all features are designated with *.*

Sandwich ELISA revealed 53.5% intact immunogenicity by the Lindmo method. Circular dichroism confirms reduced immunogenicity in terms of reduced intensity of the 210 nm trough and 220 nm peak; however, the overall shape of CD traces do not significantly change over the course of five days, suggesting intact secondary structural helicity (see Figure 6). Additionally, reduced immunogenicity is translated into ex vivo immunostaining capabilities. While murine liver sections imaged with brominated anti-TGF do show greater staining upon qualitative comparison to unstained samples, several comparisons are demonstrative of their reduced ex vivo immunogenicity. First, it is noteworthy that TGF appears to be highly distributed in both fatty and control murine liver (compare Figure 7a and 7b), suggesting that it may be too general of a target for liver fibrosis. However, brominated anti-TGF still shows lower immunostaining in fatty liver when compared to its native counterpart (compare Figure 7d against 7b) and lower immunostaining in control liver when compared to its native counterpart (compare Figure 7c against 7a). Figures 7f demonstrates that little nonspecific HRP-binding or background coloration occurs when compared to fully immunostained samples (Figures 7a –d).
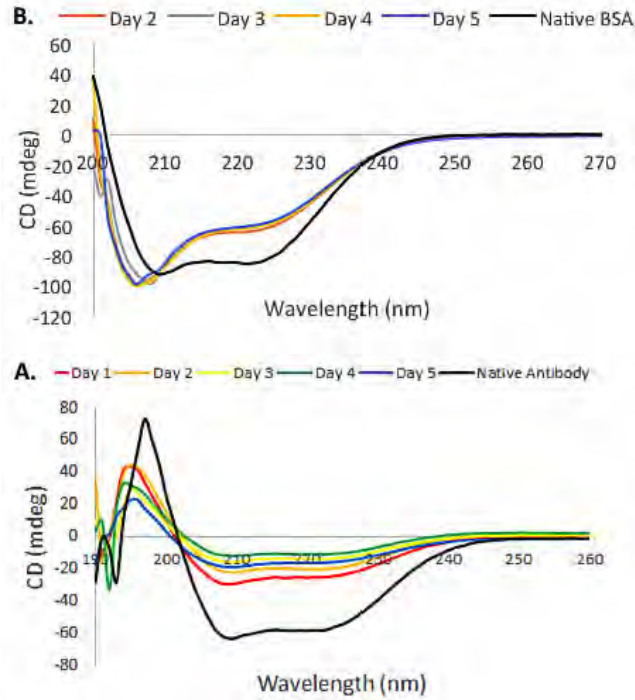
Figure 6a. *Circular dichroism profile for brominated antibody (days 1 5) in comparison to native antibody from 190 to 280 nm. Note preservation of 195 nm peak and 220 nm trough. 6b. CD profile of brominated BSA over the course of 4 days in comparison to native BSA from 200 to 280 nm. Note preservation of 207 and 222 nm troughs.*
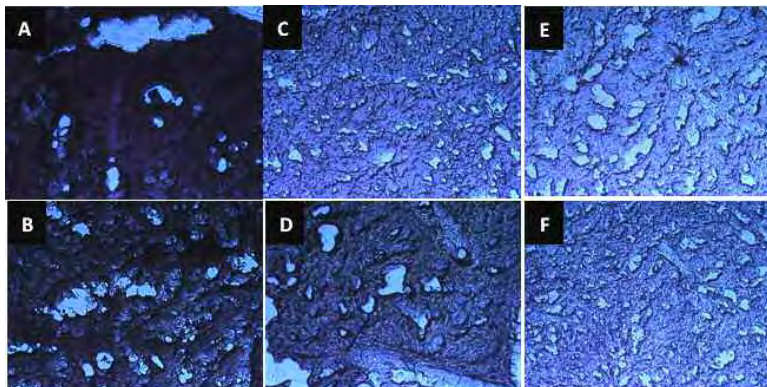

Figure 7. *Brightfield light microscope imaging of 20 µm thick murine liver slices via VIP peroxidase coloration at 10X magnification. All images taken at 0.21s exposure for qualitative comparison. A. control liver imaged with native anti-TGF showing comparative staining with B. fatty liver imaged with native anti-TGF. C. Control liver imaged with brominated anti-TGF showing lighter staining than D. fatty liver imaged with brominated anti-TGF, suggesting upregulation of TGF biomarker in fatty liver. Images compared to E. total control/unstained and F. control with only secondary horseradish-peroxidase antibody, showing little nonspecific background staining.*

3D reconstruction of NBS- and Lugol's iodine-containing capillary tubes demonstrate clear separation of both materials (see Figure 8). All tissue sections stained with Lugol's iodine did not show significant shrinkage over the time course. Sections stained for 3 and 18 hours at 0.3% Lugol's demonstrated a thin coating of iodine staining which correlated with CT imaging (see Figures 9a and b) which demonstrate only superficial attenuation with no stain penetration or visualization of tissue morphology. Staining for 6 and 30 hours at 3.0% Lugol's allowed for total tissue penetration and visualization of hepatobiliary ducts and portal system vasculature (see Figures 9c and d). 3D reconstruction of the 6 hour time point allowed for visualization of the duct and vasculature system in three dimensions (see Figure 9e). However, subsequent CT visualization of fatty liver tissue with brominated anti-TGF did not show significantly different attenuation (Figure 10) compared to control tissue under brominated anti-TGF staining conditions.
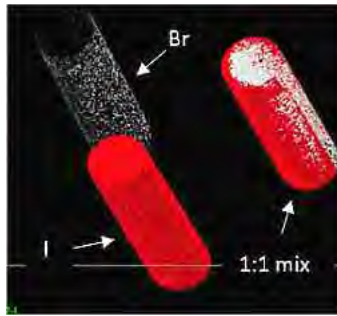

Figure 8. *3D reconstruction produced from an overlaying of binarized bromine image stacks taken at 40 kVp and binarized iodine image stacks taken at 80 kVp. 1:1 mixture shows clear separation of materials solely via eDECT.*
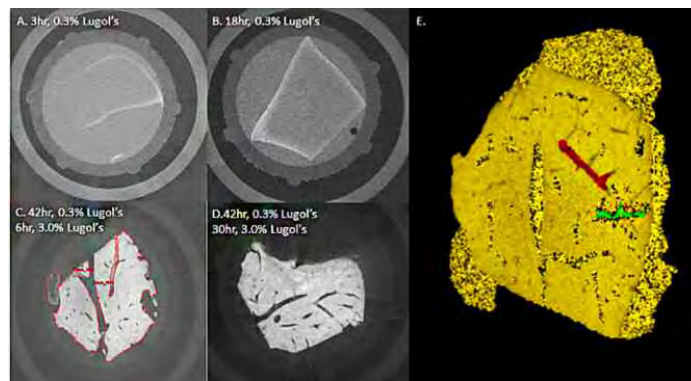
Figure 9a-b. *Cross-section along the z plane of µCT imaging of murine liver tissue under 3 and 16 hour exposure to 0.3% Lugol's iodine. Note only superficial penetration of stain. Figure 9c –d. Similar imaging of murine liver at 6 and 30 hours of exposure to 3.0% Lugol's, affording complete penetration and visualization of ducts and vasculature. All imaging performed at 70 kVp with beam hardening*
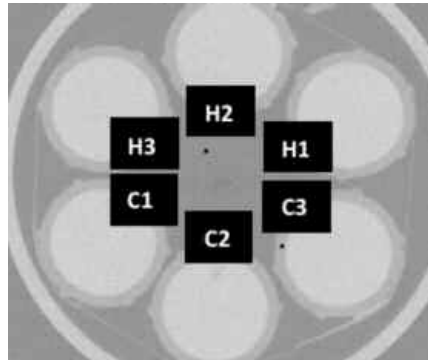
Figure 10. Cross-sectional visualization of murine tissue in agarose plugs imaged at 45 kVp with 36 µm3 isotropic voxel resolution. H1 and C1 are high fat and control tissue samples with brominated anti-TGFimmunostaining, H2 and C2 were immunostained with native anti-TGF and H3 and C3 are unstained controls.

Discussion

Our study aimed to develop a method, which allows for visualization of soft tissue morphology and separation of artifacts in 3D by first developing X-ray active brominated antibodies for key biomarkers. NAFLD murine liver served as a tissue model due to its history of qualitative and often inaccurate imaging, with TGF-β1 serving as a fibrosis biomarker for targeting. Direct bromination via oxidation yielded 36% bromination of antibody and 78% bromination of non-immunoreactive bovine serum albumin (BSA), with pH appearing to be the only factor which significantly impacts bromination yields. These yields are in line with previous reports of direct bromination via oxidation, which report $63 \pm 4\%$[22]. Although higher yields are noted for bromination of monoclonal antibodies, it should be noted that these oxidative direct brominations were carried out using a slow release of radioactive bromine with chloramine T, which has been shown to generate many fragmented protein byproducts,[23] while in this study NBS oxidation allowed for little fragmentation. Although the reported anti-TGF bromination yields are more in line with indirect bromination methods, previously reporting $49 \pm 2\%$, such methods[24] rely on the attachment of a brominated linker molecule via multistep synthesis, which lowers overall yield. In addition, with only one bromine atom per linker molecule and a single linker per antibody, signal-to-noise ratios would be markedly low for CT imaging purposes. Enzymatic bromination methods, while allowing for higher yields, require rigorous purification.[25]

Degree of bromination is determined from fourth derivative spectroscopic assays. In the original report, Bray et al. note the application of the UV method for the determination of the number of brominated tyrosyl residues in BSA via NBS oxidation and report high accuracy of tyrosyl residue determination. These factors together justified the usage of the assay. Although direct bromination targets tyrosyl residues, which may be located in antibody epitope-binding sites, 53.5% immunogenicity is still preserved in brominated antibody samples, which is quite high in comparison to the typical range of immunogenicity in oxidatively labeled IgG immunoglobulins, which ranges from 12 – 53%.[26] Furthermore, while immunogenicity is most certainly important, resulting signal-to-noise ratio is of equal importance for meaningful eDECT imaging, and if reduced immunogenicity is the result of loading 5-10 bromine atoms per antibody, it must be accepted.

Circular dichroism did reveal some structural changes to the brominated antibody. Equimolar solutions of native and brominated antibody, and for comparison BSA, did show reduced or altered attenuation at key regions, such as the 210 and 220 nm troughs. However, the overall trace, indicative of secondary structure alpha helicity, has been maintained. It should be noted that BSA profiles were not measured past 200 nm due to the effects of chloride ions in the PBS buffer on CD signal in the far-UV range.[27] If modeled after the poly-L-lysine spectrum studied by Chang, et al.[28] in which at 206.5 nm, zero β-sheet intensity is contributing to the overall signal, positive deviation in ellipticity is due to β-turns and negative deviation is due to α-helices and random coiling. Brominated antibody shows between 25-30 mdeg of positive deviation in elipticity, suggesting increasing β-turns or, more likely, a decrease in helicity due to bromination.[29]

Evidence of some structural changes reflected in CD studies and reduced in vitro immunogenicity, coincide with ex vivo immunostaining. Although brominated anti-TGF does show greater binding in fatty liver when compared to control liver also stained with brominated anti-TGF– demonstrating the upregulation of TGF in fatty liver – native anti-TGF shows greater staining in both control and fatty liver when compared to its brominated counterpart. It is possible that bromination impacted the fidelity of the primary-secondary/HRP antibody binding interaction which could reduce the degree of detection of the brominated antibody. Furthermore, it is possible that diffusion kinetics of the brominated antibody have been altered and less complete penetration of the tissue was achieved leading to poorer staining. However, support of CD and ELISA studies indicates that brominated antibody most likely has reduced immunogenicity.

Preliminary testing of dual-energy CT separation resulted in successful material separation and soft tissue visualization. It has been well established the Lugol's iodine is

a robust and flexible stain for CT visualization of soft tissue.[30] Despite previous studies demonstrating tissue shrinkage (and thus potential changes to tissue morphology) due to Lugol's staining[31], no significant difference in dry tissue mass was observed before and after staining at the 0.3 and 3.0% concentrations used. The 3.0% concentration also afforded total tissue penetration with visualization of key vasculature and duct artifacts without limiting beam hardening effects. Lugol's staining on its own was also sufficient for 3D tissue reconstruction. Additionally, when placed in the context of successful iodine and bromine separation via eDECT, Lugol's iodine serves as a robust counterstain for immuno-eDECT. However, the second component of immuno-eDECT – brominated anti-TGF – ultimately showed poor attenuation in liver tissue suggesting that the signal-to-noise ratio afforded by the degree of bromination was too low.

Conclusion and Future Direction
Our study has set out to brominate liver fibrosis biomarker anti-TGF-β 1 and test its immunogenicity while also performing preliminary demonstrations of the capabilities of immuno-eDECT. Direct methods afforded 36% bromination of anti-TGF along with reduced in vitro and ex vivo immunogenicity as well as secondary structural changes. However, direct bromination methods afforded higher immunogenicity than previously cited examples while still maintaining observable ex vivo response. In addition, separation of iodine and bromine as well as staining capabilities of Lugol's iodine demonstrate the potential robustness of immuno-eDECT. However, greater signal-to-noise of brominated antibody is required for proper CT visualization of fibrosis patterns, suggesting the need for greater degrees of bromination. This will be pursued via covalent attachment of a mainly poly-Lbromo-tyrosine moiety to anti-TGF via amine linkage which will serve as a "bromine tag." Furthermore, there is interest in tagging secondary/HRP antibodies so that immuno-eDECT may be more widely applicable to soft tissue immunostaining studies such that investigators may send a brominated secondary antibody against any primary antibody of their choice.

References
1. Wong, M.D.; Dorr, A.E.; Walls, J.R.; *Development*. **2012**, 139: 3248-56.
2. Sombke, A.; Lipke, E.; Michalik, P.; *et al., J. Comp. Neurol*. **523**, 1281-95.
3. Silva, J.M.S.; Zanette, I.; Noël, P.B.; *et al., Sci. Rep*. **2015**, 5, 14088.
4. Gignac, P.M.; Kley, N.J. *Exp. Zool. B. Mol. Dev. Evol*. **2014**, 322B: 166-76.
5. Ahnfelt-Ronne, J.; *et al., J. Histochem. Cytochem*. **2007**, 55(9): 925-930.
6. Silitoe, R.V.; *et al., J. Histochem. Cytochem*. **2002**, 50(2): 235-244.
7. Dual Energy and DSCoVer 1.0: Technical Note and Procedure. *Carl Zeiss X-Ray Microscopy*.
8. Lei, X.F.; Fu, W.; Kim-Kaneyama, J.R.; *et al., J. Hepatol*. **2016**, 64(1): 110-7.
9. Crosas-Molist, E.; Bertran, E.; Fabregat, I.; *Curr. Pharm. Des*. **2015**, 21(41): 5964-76.
10. Crosas-Molist, E.; Fabregat, I.; *Redox Bio*. **2015**, 6: 106-11.
11. Zhou, L.; Shang, M.; Shi, M.; Zhao, L.; *et al., Parasitol. Res*. **2015**. Ahead of print.
12. Li, M.; Song, J.; *et al., Human Pathol*. **2011**, 42(3): 356-60.

13. Rawlins, S.R.; El-Zammar, O.; Zinkievich, J.M.; *et al., Dig. Dis. Sci.* **2010**, 55(7): 2049-57.
14. Schwenzer, N.F.; Springer, F.; Schraml, C.; *et al., J. Hepatol.* **2009**, 51(3): 433-45.
15. Franzen, L.E.; Ekstedt, M.; Kechagias, S.; *et al., Mod. Pathol.* **2005**, 18(7): 912-16.
16. Mendler, M.H.; Bouillet, P.; Le Sidaner, A.; *J. Hepatology.* **1998**, 28(5): 785-94.
17. Raptopoulos, V.; Karellas, A.; Bernstein, J.; *Am. J. Roentgen.* **1991**, 157: 721-25.
18. Kato, Y.; et al., *Free Rad. Bio. & Med.* **2005**, 38(1): 24-31.
19. Bray, M.R.; et al., *Anal. Biochem.* **1994**, 221: 278-284.
20. Konishi, S.; *et al., Cancer Biotherapy & Radiopharm.* **2005**, 19(6): 706-715.
21. Silitoe, R.V.; Hawkes, R.; *J. Histochem. Cytochem.* **2002**, 50(2): 235-244.
22. Sundin, J.; Tolmachev, V.; Koziorowski, J.; *et al., Nucl. Med. Bio.* **1999**, 26(8): 923-29.
23. Salacinski, P.R.P.; McLean, C.; Sykes, J.E.C.; *et al., Anal. Biochem.* **1981**, 117(1): 136-46.
24. Höglund, J.; Tolmachev, V.; Orlova, A. *et al., Nucl. Med. Bio.* **2000**, 27(8): 837-43.
25. Petzold, G.; Coenen, H.H.; *Radiopharm.* **1981**, 18: 1319-36.
26. Fraker, P.; Speck, J.C.; *Biochem. Biophys. Res. Commun.* **1978**, 80(4): 849-57.
27. Tran, L.; Baars, J.; Damen, C.; *et al., Pharm. Biomed. Anal.* **2011**, 56(3): 609-14.
28. Chang, C.T.; Wu, C.S.C.; Yang, J.T.; *Anal. Biochem.* **1978**, 91: 13-31.
29. Vermeer, A.W.; Norde, W.; *Biophys. J.* **2000**, 78(1): 394-404.
30. Gignac, P.M.; *et al., J. Anat.* **2016**, 228(6): 889-909.
31. Vickerton, P.; Jarvis, J.; Jeffery, N.; *J. Anat.* **2013**, 223: 185-93.